Computational study of $LnGaO_3$ (Ln = La–Gd) perovskites

2005 J. Phys.: Condens. Matter 17 6217

(http://iopscience.iop.org/0953-8984/17/39/008)

INSTITUTE OF PHYSICS PUBLISHING JOURNAL OF PHYSICS: CONDENSED MATTER

J. Phys.: Condens. Matter **17** (2005) 6217–6234 doi:10.1088/0953-8984/17/39/008

Computational study of $LnGaO_3$ (Ln = La–Gd) perovskites

A Senyshyn[1,2], H Ehrenberg[1], L Vasylechko[2], J D Gale[3] and U Bismayer[4]

[1] Institute for Materials Science, Darmstadt University of Technology, Petersenstrasse 23, D-64287 Darmstadt, Germany
[2] Semiconductor Electronics Department, Lviv Polytechnic National University, 12 Bandera Street, 79013 Lviv, Ukraine
[3] Department of Applied Chemistry, Nanochemistry Research Institute, Curtin University of Technology, PO Box U1987, 6845 Perth, Western Australia
[4] Mineralogisch-Petrographisches Institüt, Universität Hamburg, Grindelallee 48, D-20146 Hamburg, Germany

E-mail: senyshyn@st.tu-darmstadt.de

Received 30 June 2005, in final form 19 August 2005
Published 16 September 2005
Online at stacks.iop.org/JPhysCM/17/6217

Abstract

Atomistic simulation techniques have been used to study the thermal properties of perovskite-type $LnGaO_3$ (Ln = La–Gd). A set of interatomic potentials describing interatomic interactions in these compounds was developed and tested over a wide temperature range through utilizing free energy minimization. The predicted dielectric constants, thermal expansion coefficients, phonon density of states and its projections, heat capacity and entropy, elastic moduli, Grüneisen parameters, surface energies for main crystallographic directions and Debye temperatures are in good agreement with the limited available experimental data. Perovskite-type $LnGaO_3$ (Ln = La–Gd) compounds have been examined under conditions to which substrate materials are typically subjected. Only a narrow region in the phase diagram of $LnGaO_3$ (Ln = La–Gd) and their solid solutions is recommended for use in substrate applications.

(Some figures in this article are in colour only in the electronic version)

1. Introduction

Rare-earth perovskite-type orthogallates $LnGaO_3$ (Ln = La–Gd) show a wide range of unique physical properties. Well known applications for substrate materials are for high-temperature superconductive (HTSC), colossal magnetoresistive (CMR) and GaN films [1–3]. Furthermore, $LaGaO_3$ doped with Sr and Mg, [4] as well as $NdGaO_3$ [5] and $PrGaO_3$ doped with Ca and Mg [6, 7], are promising materials for solid oxide fuel cells.

The determination of the thermal behaviour of the structure of $LnGaO_3$ compounds for non-ambient conditions began with low-temperature (LT) studies of $LaGaO_3$, $PrGaO_3$ and

$NdGaO_3$ at 12 K by neutron powder diffraction [8–12]. Recently, information about the thermal behaviour of these compounds was supplemented by structural investigations using high-resolution powder diffraction obtained using synchrotron radiation, in the temperature range 12 K–RT (room temperature) [13]. The high-temperature (HT) structure evolution of $LaGaO_3$ has been investigated intensively [10, 14–16] mainly because of the existence of a structural phase transition. The HT structures of neodymium and praseodymium orthogallates studied using synchrotron powder diffraction were reported earlier in [17, 18]. Anisotropy of $NdGaO_3$ thermal expansion was studied in [19] by x-ray powder diffraction and its relationship to the crack formation in $YBa_2Cu_3O_{7-\delta}$ has been determined and discussed. The crystal structure of $CeGaO_3$ was described either as tetragonal [20, 21] (space group $P4/mmm$) or orthorhombic [22] (space group $Pbnm$). Examinations of its structure using high-resolution powder diffraction with a high signal-to-noise ratio revealed that $CeGaO_3$ possesses an orthorhombically distorted $GdFeO_3$-type structure over the whole temperature range investigated (12–1170 K) [23–25].

In the literature, there are no thermal structure data available for $LnGaO_3$ with Ln heavier than Nd. The main reason is that $LnGaO_3$ with Ln^{3+} ionic radii smaller than the Nd radius (Ln = Sm–Lu) can be hardly obtained by solid-phase synthesis methods at ambient pressure, because the corresponding garnet ($Ln_3Ga_5O_{12}$) and $Ln_4Ga_2O_9$ phases are formed preferentially. In [26], the synthesis by arc melting of a product with 57 wt% of $SmGaO_3$ perovskite phase ($GdFeO_3$-type structure) at RT has been reported (but also, the presence of 27 wt% of garnet $Sm_3Ga_5O_{12}$ and 16 wt% of a $Sm_4Ga_2O_9$ phase were detected). Following [27], in the $Nd_{1-x}Sm_xGaO_3$ solid solutions the pure perovskite phase is limited to 75–90 mol% of Sm, whereas in the pseudobinary systems $LaGaO_3$–$SmGaO_3$ [28, 29] and $LaGaO_3$–$GdGaO_3$ [30] the pure perovskite phases are limited by ∼70 and ∼50 mol% of Sm and Gd, respectively.

The main reason for the preferred formation of $Ln_3Ga_5O_{12}$ and $Ln_4Ga_2O_9$ could be the decrease of the Ln ionic radii with increasing atomic number and, therefore, octahedral site occupation by Ln ions [31]. Thus, inter-lanthanide perovskites are known from the literature ($LaDyO_3$, $LaYO_3$, $LaHoO_3$, $LaErO_3$) [32, 33], where Ln ions with the larger ionic radii (La, Ce, Pr) occupy the cuboctahedral sites, whereas Ln ions with smaller ionic radii have octahedral coordination. Levy *et al* [34] reported a decrease of the antisite reaction energy for $LnGaO_3$ when Ln ionic radii decreases.

Two methods for obtaining pure perovskite-type $LnGaO_3$ (Ln = Sm–Lu) compounds have been developed:

- decomposition of the corresponding garnet phases at high temperatures and pressures (4.5 GPa, 1300 K) over a NaOH melt; [35]
- overheating of $0.5Ln_2O_3$–$0.5Ga_2O_3$ (Ln = Sm–Er) melts [36].

In particular, Marezio *et al* [35] ascribed the $GdFeO_3$ structure type and determined corresponding lattice parameters for all $LnGaO_3$ at RT, except $PmGaO_3$, for which structural properties are unknown so far. Nevertheless, for the perovskite-type orthogallates $LnGaO_3$ with Ln heavier than Sm the structure has only been determined in detail for $GdGaO_3$ and at RT [37]. Established methods have been found unsuccessful in obtaining sufficiently large single crystals of high quality.

The purpose of this study is to develop a computational model that could be used in order to predict structural and other physical properties of orthorhombic perovskite-type rare-earth gallates, including $PmGaO_3$, as well as to determine the region of the structural stability of $LnGaO_3$ perovskites. Moreover, following reference [38], materials with the $GdFeO_3$-type structure are the most common ones in the wide family of perovskites. Therefore, an

improved knowledge of the structure–property relationship is an objective of general interest for this class of structures, particularly with respect to the major utilization of these materials as substrates in devices operated between liquid nitrogen temperature and RT. In order to determine the temperature-dependent physical behaviour in this regime, quasiharmonic lattice dynamics simulations, based on the free energy minimization technique, have been applied.

2. Methodology

The atomistic simulation method is based on the Born model of solids where interatomic potential functions are defined to simulate the long-range attractive and short-range repulsive forces acting between the constituent ions of a solid.

Long-range forces are described by Coulomb's law and typically dominate the lattice energy, while the analytic form of the potential used to describe short range interactions depends on the character of the bonding in the material of interest.

In the literature, there are several sets of potential parameters that contain the necessary interatomic interactions to describe the present family of compounds [39–45]. Many of these models were developed through the fitting of multiple oxides to enhance their transferability. While this practice is often reasonably successful for simpler materials, it will compromise the accuracy of the description of a specific family of more complex materials. When phases are being studied with phase transitions to lower symmetries [46], as for the case of orthorhombic $LnGaO_3$ perovskites, the results are especially sensitive to the model parameters, and in particular the oxide ion polarizability.

Special note should be given to the set of potential parameters derived in [34] describing Ln–O (Ln = La–Lu, Sc, Y) and Me–O (Me = Al, Cr, Ga, Fe, Sc, In) interactions in rare-earth metal oxides with perovskite and bixbyite structures. Studying the tolerance of these materials to radiation damage, the authors considered lattice energies and processes driven by the Schottky, oxygen Frenkel, and antisite defect reaction mechanisms as well as their relationship to cation sizes.

Most of the above-cited potential models were fitted using athermal calculations (i.e. the effect of temperature is implicitly included in the fitted parameters). In the present study, temperature is explicitly included, and, hence, it was necessary to refine the existing potentials [18, 47] and derive new parameters for modelling perovskite-type $LnGaO_3$.

2.1. Structure data construction

From the literature the atomic positions within the unit cell at RT are known for $LaGaO_3$, $CeGaO_3$, $PrGaO_3$, $NdGaO_3$, $SmGaO_3$ and for $GdGaO_3$. Previously, Marezio *et al* [35] reported only lattice parameters for all $LnGaO_3$ at RT, except $PmGaO_3$. Nevertheless, not only are the lattice parameters necessary for the construction of the interaction model, but the atomic positions within the cell also. In order to obtain information about atomic positions in the cell at RT for $PmGaO_3$ and $EuGaO_3$, we decided to apply an interpolation procedure to the existing structural data of $LnGaO_3$ and their set of their solid solutions at RT [26–30, 48–52]. The $LnGaO_3$ perovskites show an increase of deformation of the perovskite cell with respect to the ideal perovskite as the Ln atomic number increases, as is indicated by the Goldschmidt tolerance factor t

$$t = \frac{r_{\mathrm{Ln}} + r_{\mathrm{O}}}{\sqrt{2}(r_{\mathrm{Ga}} + r_{\mathrm{O}})}. \tag{1}$$

This well known geometrical relationship is unity for a deformation of the perovskite structure if the lattice is treated as an array of close-packed spheres, where r_{Ln}, r_{Ga} and r_{O} are the ionic

Table 1. Experimental structural parameters of $LnGaO_3$ at room temperature. The space group is *Pbnm* (No. 62). The structural data were modelled for Ln and O1 ions occupying the 4c position with $z = 1/4$, Ga occupies the position 4b [1/2, 0, 0]. Numbers in parentheses give statistical errors in the last significant digit.

Parameters		$LaGaO_3$ [15]	$CeGaO_3$ [23]	$PrGaO_3$ [17]	$NdGaO_3$ [54]
	a (Å)	5.524 5(1)	5.490 9(1)	5.455 7(1)	5.427 6(1)
	b (Å)	5.492 2(1)	5.485 7(1)	5.490 1(1)	5.497 90(9)
	c (Å)	7.774 0(2)	7.748 2(2)	7.727 5(2)	7.707 8(1)
Ln, 4c	x/a	−0.004 1(3)	−0.005 9(4)	−0.007 42(2)	−0.009 10(4)
	y/b	0.016 8(3)	0.027 6(2)	0.035 22(3)	0.041 42(4)
O1, 4c	x/a	0.066 9(3)	0.067(3)	0.075 8(4)	0.080 0(5)
	y/b	0.494 2(4)	0.494(2)	0.484 8(4)	0.482 6(5)
O2, 8d	x/a	−0.270 1(3)	−0.289(3)	−0.286 8(2)	−0.289 3(3)
	y/b	0.270 4(3)	0.275(3)	0.287 1(2)	0.290 3(3)
	z/c	0.035 6(2)	0.037(2)	0.040 4(2)	0.042 2(2)
Parameters		$PmGaO_3$ [a,b]	$SmGaO_3$ [26][b]	$EuGaO_3$ [a,c]	$GdGaO_3$ [37][c]
	a (Å)	5.396 63	5.378 09(5)	5.351	5.322
	b (Å)	5.507 77	5.516 61(6)	5.528	5.537
	c (Å)	7.677 71	7.655 01(8)	7.628	7.606
Ln, 4c	x/a	−0.011 21	−0.013 1(3)	−0.013 77	−0.014 70(5)
	y/b	0.047 65	0.049 8(2)	0.055 05	0.059 33(5)
O1, 4c	x/a	0.085 44	0.089(2)	0.091 51	0.095 02(85)
	y/b	0.475 98	0.474(2)	0.472 95	0.472 35(86)
O2, 8d	x/a	−0.292 91	−0.295(2)	−0.296 76	−0.300 01(57)
	y/b	0.286 76	0.288(2)	0.289 57	0.298 87(60)
	z/c	0.044 73	0.045 9(13)	0.047 28	0.049 13(47)

[a] Lattice parameters and/or
[b] Atomic positions deduced from polynomial fit.
[c] Lattice parameters from [35].

radii of Ln, Ga and O, respectively. Taking into account the conformity of Ln properties, at least in Ce or Gd subgroups of rare-earth elements, the different properties could be analysed from the degree of the perovskite cell deformation.

Shannon [53] has tabulated ionic radii for chemical elements in a variety of coordination environments and oxidation states, and these have been found to be applicable in the case of perovskite-type $LnGaO_3$. In the ideal situation, equation (1) requires radii in a 12-fold coordination environment, but unfortunately 'cuboctahedral' radii are not available for the whole set of Ln^{3+} ions. Lufaso *et al* [38] have used an extrapolation procedure to estimate the missing values. Nevertheless, qualitatively similar behaviour has been observed for the Goldschmidt tolerance factor dependences calculated using rare-earth ionic radii in cuboctahedral and nine-fold coordination environments. Therefore, instead of using the Goldschmidt tolerance factor for analysing the properties of $LnGaO_3$ as a function of the perovskite cell deformation, we decided to use the Ln^{3+} ionic radii in the nine-fold coordination environment tabulated by Shannon for all rare-earth elements.

Estimated structure parameters of $PmGaO_3$ and $EuGaO_3$, along with experimental data for La, Ce, Pr, Nd, Sm and Gd orthogallates, are summarized in table 1 as structural input data for further calculations (*vide infra*). Modelling of $LnGaO_3$ with Ln heavier than Gd requires more accurate information about the structural and other properties of these compounds. Consequently, simulations were only performed up to $GdGaO_3$.

2.2. Potential derivation

Similarly to references [18, 47], in the present work we used only pair potentials. Simulations were carried out in an ionic approximation and the Buckingham form of potential has been chosen according to

$$U_{ij}(r) = \frac{Z_i Z_j e^2}{r} + A_{ij} \exp\left(-\frac{r}{R_{ij}}\right) - \frac{C_{ij}}{r^6}, \tag{2}$$

where the individual terms describe the Coulomb potential, the Born–Mayer repulsion and the dispersion interactions, respectively. Here r is the interatomic distance between atoms i and j, Z_i is the effective charge of the ith atom, the A_{ij}, R_{ij} and C_{ij} are the short-range potential parameters for each pair of atoms, usually determined based on a fit to experimental data.

For oxygen–oxygen interactions we used parameters of the interaction potential and of the shell model reported by Lewis *et al* [41] We neglect the short-range contribution to the cation–cation interactions since the cations tend to be contracted, leading to negligible overlap of electron density, and of low polarizability, leading to only a small contribution of van der Waals attraction. Similarly, we neglected the dispersion term for the cation–anion interactions, again due to the relative small polarizability of the cations. The errors associated with these approximations will be subsumed into the fitted values of the remaining parameters. Assuming the potentials to be transferrable, we considered the oxygen–oxygen and gallium–oxygen interatomic potentials as common for all considered $LnGaO_3$ compounds. Consequently, only the rare-earth–oxygen and a single common gallium–oxygen interaction need to be determined.

An appropriate potential to describe the Ga–O interactions was derived from the following experimental data:

- $NdGaO_3$ structure at 100 K, measured using high-resolution single-crystal diffraction of synchrotron radiation [54];
- full elastic constant tensor measured by an ultrasonic method at 77 K [55];
- average static dielectric constant at 100 K [56].

As a first approximation, we used the results for fitting interactions in $NdGaO_3$ and $Nd_{0.75}Sm_{0.25}GaO_3$ [18, 47]. For derivation of the Ln–O interactions, we used the experimentally determined and estimated structures of $LnGaO_3$ (Ln = La–Gd) at RT (table 1). As a starting point for refinement, the parameters obtained from fitting to the structures of the respective simple oxides Ln_2O_3 were taken from the ICSD database [57].

Structural data for every $LnGaO_3$ (Ln = La–Gd) phase were fitted separately using the 'relax' fitting technique and free energy minimization [58] within the GULP (General Utility Lattice Program) code [59, 60]. The study is performed using the zero static internal stress approximation, in which the internal variables are optimized with respect to the internal energy, whilst only the strain variables are optimized with respect to the free energy. Potential cut-off radii were assumed to be a 12 Å for all interactions. For the Brillouin zone integration of the phonon density of states, the scheme of Monkhorst and Pack [61] with an $8 \times 8 \times 8$ grid of points in reciprocal space was used. The best agreement between experimentally determined and calculated properties was obtained with the interaction parameters summarized in table 2. The deviations between calculated and input lattice parameters, as well as cell volumes, were smaller than 1% for all $LnGaO_3$ considered, which is reasonable for such force field simulations.

Parameters of the Born–Mayer repulsion A_{ij} and R_{ij} (equation (2)) for different rare-earth–oxygen interactions are shown in figure 1. Obtained results illustrate convincingly the so-called 'lanthanide stiffness' effect, where the atomic radii of the rare-earth elements decrease

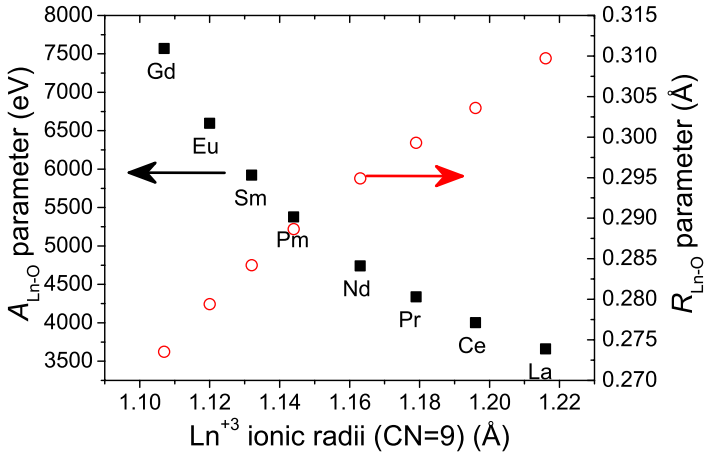

Figure 1. Derived parameters of the Born–Mayer repulsion for different pairs Ln–O (Ln = La–Gd).

Table 2. Parameters of the derived interatomic interactions (equation (2)).

Pair of atoms	A_{ij} (eV)	R_{ij} (Å)
La^{3+}–O^{2-}	3382.07	0.314 65
Ce^{3+}–O^{2-}	3979.43	0.304 12
Pr^{3+}–O^{2-}	4314.82	0.299 77
Nd^{3+}–O^{2-}	4690.67	0.295 57
Pm^{3+}–O^{2-}	5311.29	0.289 38
Sm^{3+}–O^{2-}	5846.88	0.284 89
Eu^{3+}–O^{2-}	6493.28	0.280 18
Gd^{3+}–O^{2-}	7166.76	0.275 81
Ga^{3+}–O^{2-}	551.66	0.383 63

with increasing numbers of electrons (similar to the behaviour of the R_{ij} and A_{ij} parameters of the Born–Mayer type of repulsion).

3. Results and discussion

In [62] O'Bryan *et al* proposed several criteria for substrate materials in HTSC electronic applications, in addition to the standard condition of a minimum in the mismatch between the cell parameters of deposited film and substrate. In this section, the satisfaction of the conditions of O'Bryan *et al* is controlled by analysing available experimental data and calculated properties of $LnGaO_3$.

3.1. Dielectric properties

The first requirement for HTSC applications is a low dielectric loss. Additionally, the authors of [63] lay down further conditions for the dielectric properties of substrates for HTSC films:

- $\tan\delta \leqslant 10^{-4}$;
- if $\varepsilon \leqslant 10$ substrate utilization is permitted in HTSC microwave integrated circuits with an operating frequency above 10 GHz;

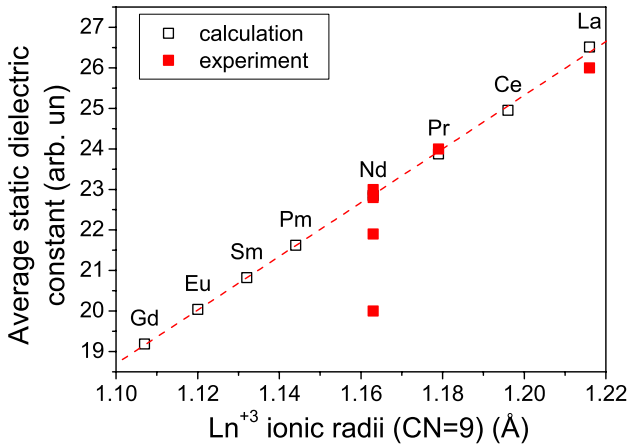

Figure 2. Comparison of calculated and experimental dielectric constants of different $LnGaO_3$ (Ln = La–Gd) at RT as function of Ln^{3+} ionic radii (here and below dashed lines in the figures are given as a guide for the eye).

- if $\varepsilon \leqslant 25$ substrate utilization is permitted in HTSC microwave integrated circuits with an operating frequency below 10 GHz.

Moreover, during calculations the dielectric constant tensor depends on the inverse second derivative matrix; it has many of the characteristics of the Hessian matrix, and is therefore quite a sensitive indicator of whether a potential model is physically reasonable, as well as whether the present structure is a genuine local minimum [64].

Unfortunately, the dielectric losses of $LnGaO_3$ have not been well studied yet. However, comparing available data on gallates one may expect the loss tangent to be lower than 10^{-4} at 10 GHz and 77 K, except for compounds with Nd^{3+} in $4f^3$ configurations as a constituent, where the thermal behaviour of tan δ as well as ε has been found to be somewhat atypical for dielectrics [56, 65–67]. We were unable to simulate this anomaly using atomistic modelling, which could be an indicator of its electronic nature.

Results of our calculations of ε at RT, presented in figure 2, show a practically linear decrease with decreasing Ln^{3+} ionic radii (equivalent to an increasing of the Ln^{3+} atomic number). A similar dependence was reported for orthorhombic $LnAlO_3$ in [68], where microwave properties were studied experimentally. Results of our calculations agree well with the experimental observations [56]. For $LaGaO_3$ a low-frequency dielectric constant of ∼26 [2, 69] has been reported, while for $PrGaO_3$ ε it is equal to ∼24 [70] and for $NdGaO_3$ $\varepsilon \sim$ 20–23 [65–67, 71, 72].

3.2. Thermal expansion

The next criterion of O'Bryan *et al* [62] is the condition of similarity between thermal expansion coefficients (TECs) for the substrate and deposited material. The volumetric TEC α_V can be expressed as [73]

$$\alpha_V = \frac{\gamma_V \rho C_V}{K_T} = \frac{\gamma_V \rho C_P}{K_S}, \tag{3}$$

where γ_V is the Grüneisen parameter, ρ is the density of material, K_T and K_S are isothermal or adiabatic bulk moduli, and C_V and C_P are the heat capacities at constant volume and pressure

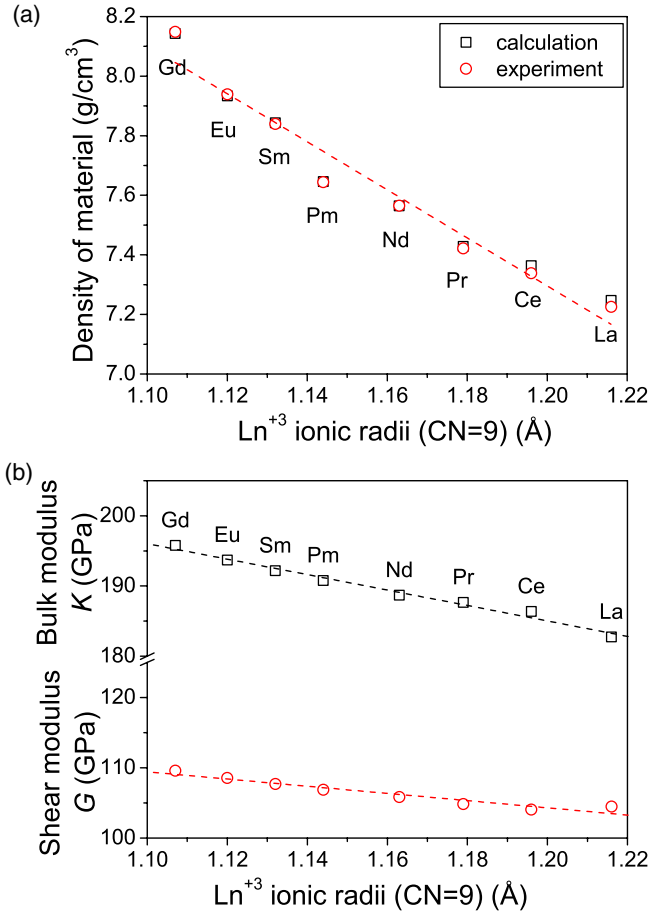

Figure 3. Density of $LnGaO_3$ (Ln = La–Gd) (a) and their bulk and shear moduli (b) at RT as a function of Ln^{3+} ionic radii.

respectively. In the following we consider the terms of equation (3) in detail. Firstly, let us analyse the density of $LnGaO_3$ and its elastic properties.

3.2.1. Density of $LnGaO_3$ and its elastic properties. Calculated densities ρ of $LnGaO_3$ are presented in figure 3(a) and compared with x-ray densities obtained from the cell volumes (table 1). Good agreement between calculated and x-ray densities are in line with the previously reported consistency between calculated and experimental cell volumes (within 1% of error as mentioned above).

Elastic constants were calculated as second derivatives of the energy density with regard to external strain. The elastic moduli were obtained using the Reuss–Voigt–Hill averaging scheme for the tensor of elastic constants. Calculated values, presented in figure 3(b), increase with increasing Ln atomic number, which correlates well with the results of sclerometric measurements reported in [74], i.e. increasing of the Mohs hardness in $LnGaO_3$ as Ln changes from La to Sm.

For measurement of elastic constants, sufficiently large and high-quality single crystals are required, which explains the lack of data in the literature concerning the elastic properties

of $LnGaO_3$. Results of ultrasonic measurements were only reported for $NdGaO_3$ at 77 K ($K = 190.0$ GPa, $G = 92.4$ GPa) [55]. The bulk modulus of $NdGaO_3$ at RT calculated in this work ($K = 188.7$ GPa) shows good agreement with the experimental value of Krivchikov *et al* [55], whereas for the shear modulus ($G = 105.8$ GPa) a pronounced difference is found. The bulk modulus of $LaGaO_3$ was estimated to be equal to 165 ± 32 GPa from the V–P data [75] using the second-order Birch–Murnaghan equation of state.

3.2.2. Debye temperature. The Debye model is not an appropriate description for the thermal behaviour of $NdGaO_3$ and the $Nd_{0.75}Sm_{0.25}GaO_3$ structure [18, 47]. The heat capacity is only well reproduced by the Debye model below 100 K, where acoustic phonons play an important role; the Grüneisen parameter and TEC are calculated to be about 35% lower than experimentally observed.

Nevertheless, the Debye temperature remains important for the characterization of the overall thermodynamic behaviour of the crystal, at least at $T \leqslant \theta_D/10$. Overestimation of the calculated shear modulus leads to the overestimation of the calculated Debye temperature, as determined by the Robie and Edwards relation [76]

$$\theta_D = \frac{\hbar}{k_B}\left(\frac{6\pi^2 nN}{V}\right)^{\frac{1}{3}}\left[\frac{1}{3}\left(\frac{3K+4G}{3\rho}\right)^{-\frac{3}{2}} + \frac{2}{3}\left(\frac{G}{\rho}\right)^{-\frac{3}{2}}\right]^{-\frac{1}{3}}, \tag{4}$$

where $\hbar$ and k_B are Planck's and Boltzmann's constants respectively, n is the number of atoms per formula unit, N is the number of formula units per cell and V is the cell volume. Debye temperatures, calculated via equation (4), are presented in figure 4(a). We supposed that the observed difference is associated with the overestimation of the shear modulus calculated, for which equation (4) is more sensible than to the bulk modulus. Krivchikov *et al* [55] reported $\theta_D = 514.2$ K for $NdGaO_3$ at $T = 77$ K. Furthermore, by analysing the isotropic atomic displacement parameters [18], the athermal Debye temperature of $NdGaO_3$ has been estimated to be 510 ± 27 K. Our present calculations yield a value of 550 K for $NdGaO_3$ at RT.

3.2.3. Phonon and thermodynamic properties. By analysing the phonon density of states in $LnGaO_3$ it was also concluded that rare-earth, gallium and oxygen atoms dominate the phonon spectrum in different frequency regions. Moreover, the region of the Ln^{3+} contribution to the total phonon density of states in $LnGaO_3$ is systematically shifted to the low-frequency side with increasing Ln^{3+} atomic number (and, respectively, its atomic weight), which could be an explanation of the observed decreasing of Debye temperatures, thermodynamic properties, Grüneisen parameter and TECs.

Heat capacities, entropies and Grüneisen parameters of $LnGaO_3$ (Ln = La–Gd) at RT were calculated from the obtained phonon spectrum as described in [18, 47, 77] and shown in figures 4(a), (b) and 5(a), respectively. Results of our calculations correlate well with the experimental heat capacities at constant pressure C_P (at RT for $LaGaO_3$ $C_P = 440$ J mol^{-1} K^{-1}; for $NdGaO_3$ $C_P = 423$ J mol^{-1} K^{-1}) [78, 79], but show a ca ~8% lower value, which is reasonable taking into account that C_P is usually higher than C_V by

$$C_P - C_V = \frac{\alpha^2 K_T T}{\rho}. \tag{5}$$

Another reason for the observed differences is the contribution to C_P caused by crystal field–electronic subsystem interactions, which is relevant in compounds containing rare-earth elements.

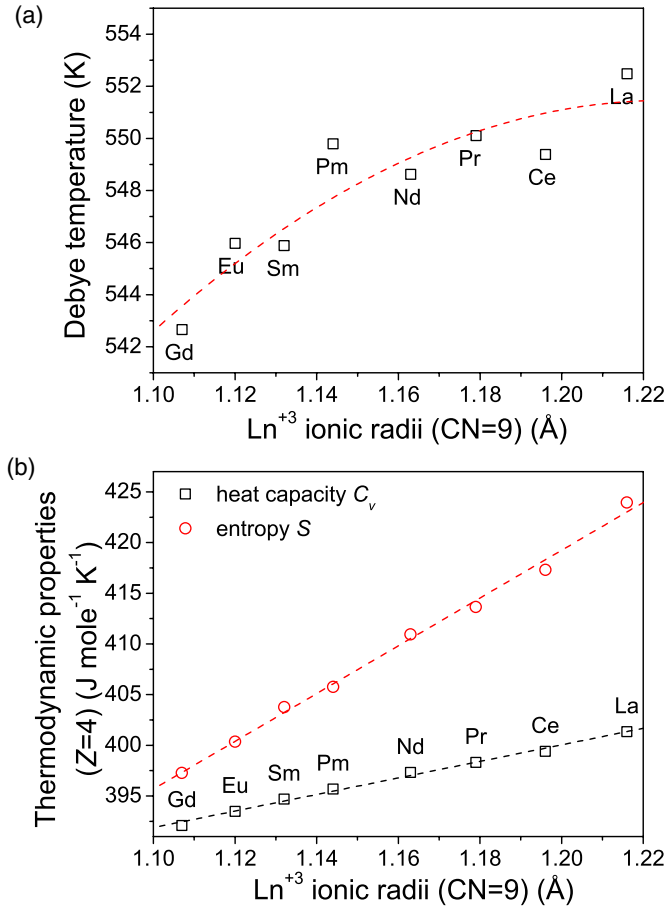

Figure 4. Debye temperature (a) and thermodynamic properties (b) of $LnGaO_3$ (Ln = La–Gd) at RT as a function of Ln^{3+} ionic radii.

Volumetric thermal expansion coefficients were calculated from the available V–T data using

$$\alpha_V = \frac{\partial \ln[V(T)]}{\partial T}, \tag{6}$$

where the volume of the relaxed cell is $V(T)$. Calculated TECs for $LnGaO_3$ are presented in figure 5(b).

For comparison of calculated and experimental TECs we reconstructed the $V(T)$ dependence from the known $\alpha_V(T)$ using the V–T equation of state

$$V_T = V(T_0) \exp\left[\int_{T_0}^{T} \alpha(t)\, dt\right] \tag{7}$$

and compared these dependences to the experimentally observed $V(T)$ data.

For $LnGaO_3$ (Ln = La–Nd), the known experimental cell volumes at 12 K have been used as $V(T_0)$, whereas for prediction of the thermal evolution of the cell volumes for other $LnGaO_3$ (Ln = Pm–Gd) we solved equation (7) with known V(RT) (table 1). Figure 6 illustrates the agreement between the experimentally observed thermal evolution of cell volume (presented

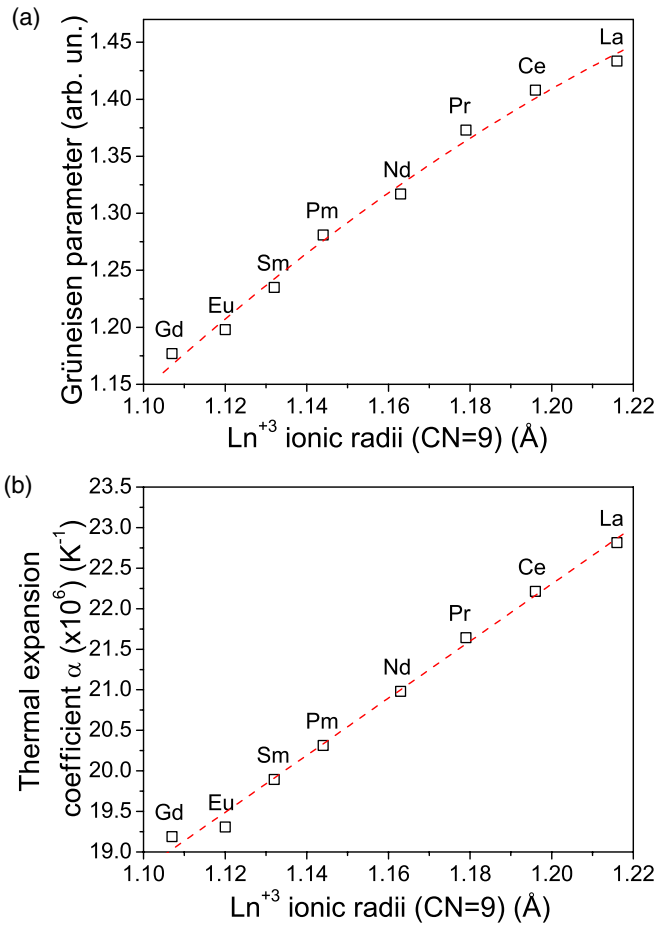

Figure 5. Grüneisen parameters (a) and TECs (b) of $LnGaO_3$ (Ln = La–Gd) at RT as a function of Ln^{3+} ionic radii.

by points) [13, 17, 18, 23, 24] and cell volumes calculated using equation (7) (lines). The distinctive bends in the HT region of the calculated $V(T)$ we associate with the failure of the quasiharmonic approximation, which is unable to describe the large atomic displacements, which occur at HT.

We were not able to simulate the negative thermal expansion in $PrGaO_3$ at low temperatures, as reported in [13, 17]. Primarily it is assumed to be an indication of crystal field effects, since semiclassical methods are unable to simulate electronic properties, which are entirely in the domain of study by *ab initio* methods. We suppose that the negative thermal expansion observed for $PrGaO_3$ and $La(Pr)GaO_3$ [13, 17, 27] is associated with interactions between phonon modes of GaO_6 polyhedra with the electronic levels of a Pr^{3+} ion in the crystal field. Additional studies about this anomaly are in progress.

3.3. Phase transitions and stability

A final criterion of O'Bryan *et al* [62] for good substrate materials requires the absence of structural phase transitions, not only in the temperature region of film deposition, but also

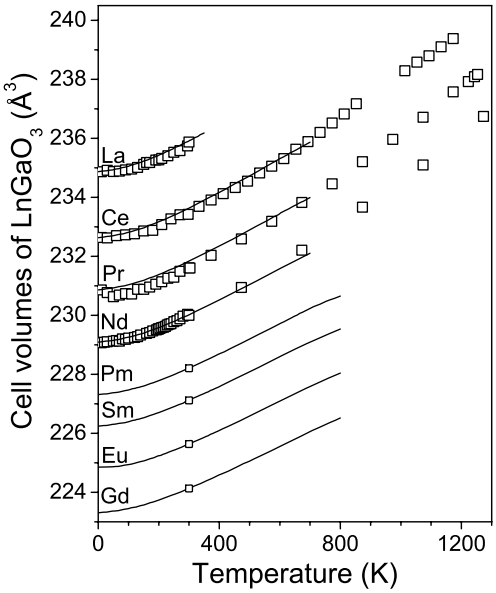

Figure 6. Thermal dependence of $LnGaO_3$ (Ln = La–Gd) cell volumes. The experimental data are shown by points; the lines are the results of our calculations.

below the melting point of the substrate material in order to suppress the formation of micro-twins and roughness of the substrate surface [80]. Chosen methodology of simulations cannot be considered as good tool for modelling of high-temperature behaviour of solids as well as their structural transformations, therefore in this section the only available literature data were analysed.

Lanthanum gallate $LaGaO_3$ undergoes a $Pbnm$–$R\bar{3}c$ first-order structural phase transition between 418 and 423 K [2, 62, 81], and no rhombohedral–cubic phase transformation was detected up to 1673 K [15]. Using calorimetric studies the $Pbnm$–$R\bar{3}c$ phase transition in $CeGaO_3$ has been detected at 1228 K [23, 24]. For the determination of T_c of the $Pbnm$–$R\bar{3}c$ phase transition in $PrGaO_3$ three independent techniques were used for its estimation [17]. The existence of the $R\bar{3}c$ phase in a small temperature range below its melting temperature has been concluded, which is in agreement with an experiment of Sasaura *et al* [82]. For $NdGaO_3$ no structural phase transitions were detected up to its melting point [83, 84]. Furthermore, a set of transition temperatures has been reported already for the systems $La_{1-x}Pr_xGaO_3$ [51], $La_{1-x}Nd_xGaO_3$ [50], $La_{1-x}Sm_xGaO_3$ [29], $La_{1-x}Gd_xGaO_3$ [85] and $La_{1-x}RE_xGaO_3$ (RE = Ce, Sm, Ho, Er, Y) [17]. Temperatures for the phase transition show a practically linear behaviour as a function of the perovskite-cell deformation. The data from the above cited reference are shown in figure 7 by open points; the dotted line represents a linear fit, and the solid line is a linear fit of experimentally determined melting temperatures [86–89] (presented by filled squares). The crossover point of the results of interpolation determines the value of a critical perovskite-cell deformation (in units of Ln^{3+} ionic radii) leading to the $Pbnm$–$R\bar{3}c$ phase transition. Thus, for $LnGaO_3$ and their solid solutions with average ionic radii in a nine-fold coordination sphere greater than ∼1.177 Å, the $Pbnm$–$R\bar{3}c$ phase transition is expected to occur and, hence, a strong tendency to twinning can be assumed.

There is, however, a problem in obtaining high-quality single crystals with an average Ln ionic radii smaller than that of Nd (1.163 Å). The mechanism of this instability is

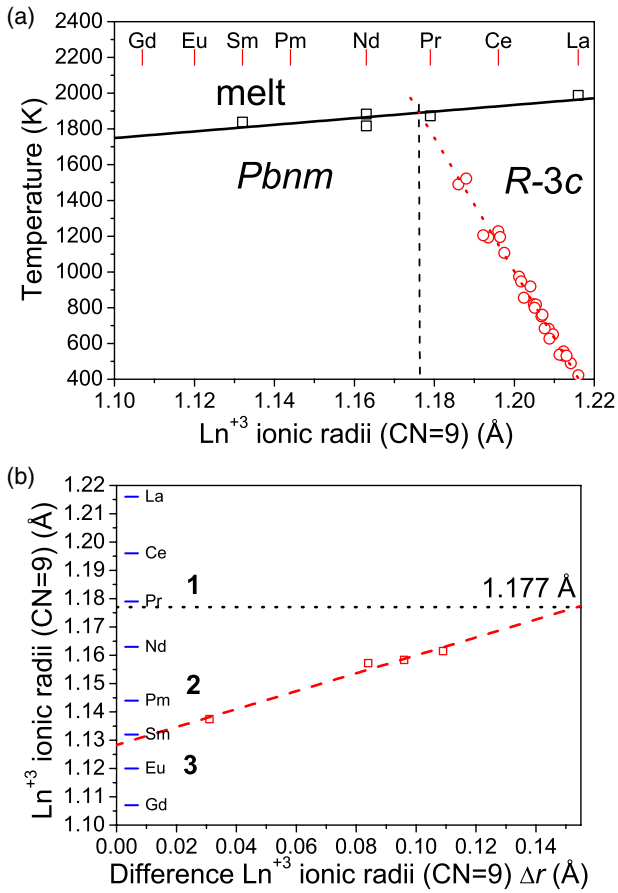

Figure 7. Generalized phase diagram of perovskite-type $LnGaO_3$ (a). Data from [86–89] correspond to melting points (squares). Transition temperatures (circles, [2, 17, 23, 24, 29, 50, 51, 62, 81, 85]) increase linearly up to 1.177 Å. Stability diagram of perovskite-type $LnGaO_3$ (b). The region 1 describes materials that undergo a $Pbnm$–$R\bar{3}c$ phase transition below their melting; materials belonging to region 3 can be synthesized by applying high-pressure; region 2 describes the range of compositions for potential substrate materials.

not well understood and can be associated with increased distortion of oxygen polyhedra when rare-earth ionic radii decrease. Oxygen polyhedra become more regular by applying pressure [90, 91], which explains the successful high-pressure synthesis of $LnGaO_3$ containing rare-earths of the Gd subgroup. Therefore, we approached the critical composition value (critical deformation of the perovskite cell in terms of ionic radii r_{cr}) for the $LnGaO_3$ (Ln = La–Gd) system, which separates the structures synthesized either at ambient pressure or at high pressures. The solid solutions $La_{1-x}Gd_xGaO_3$, $La_{1-x}Eu_xGaO_3$, $La_{1-x}Sm_xGaO_3$ and $Nd_{1-x}Sm_xGaO_3$ are limited by x equal to about 0.5, 0.6, 0.7 and 0.9, respectively, or in the terms of average rare-earth ionic radii by 1.162, 1.158, 1.157 and 1.137 Å. Clearly visible differences between obtained boundary compositions (in terms of average rare-earth ionic radii) indicate the limitations for the general assumption of a critical deformation. Therefore, other factors should be included in these considerations.

Following [92], continuous (long) solid solutions could be formed if differences in the sizes of substituted constituents are not greater than 15%. As a first approximation,

Table 3. Estimated regions of stability for perovskite-type $LnGaO_3$ and their solid solutions. (Note: R_1 and R_3 in the table mean that the respective pseudobinary system lies entirely within region 1 or region 3.)

Ln	La	Ce	Pr	Nd	Pm	Sm	Eu	Gd
La	R_1	R_1	R_1	0.74–1.00	0.54–1.00	0.46–0.73(3)	0.41–0.60(3)	0.36–0.49(3)
Ce		R_1	R_1	0.58–1.00	0.37–1.00	0.30–0.74(4)	0.25–0.57(4)	0.21–0.44(3)
Pr			R_1	0.13–1.00	0.06–1.00	0.04–0.76(6)	0.03–0.54(5)	0.03–0.39(4)
Nd				0.00–1.00	0.00–1.00	0.00–0.80(9)	0.00–0.49(7)	0.00–0.30(5)
Pm					0.00–1.00	0.00–1.0(2)	0.00–0.3(1)	0.00–0.11(8)
Sm						R_3	R_3	R_3
Eu							R_3	R_3
Gd								R_3

the total deformation r_{tot} of the perovskite cell under Ln substitution (in terms of average rare-earth ionic radii) could be presented as a superposition of a critical deformation value and differences between the rare-earth elements Δr in the pseudobinary system $Ln1GaO_3$–$Ln2GaO_3$ (Ln1, Ln2 = La–Gd)

$$r_{tot} = r_{cr} + k\Delta r. \tag{8}$$

The r_{cr} and k values have been found by fitting of average Ln ionic radii for $La_{0.5}Gd_{0.5}GaO_3$, $La_{0.6}Eu_{0.4}GaO_3$, $La_{0.7}Sm_{0.3}GaO_3$ and $Nd_{0.1}Sm_{0.9}GaO_3$ to equation (8). The generalized phase diagram (figure 7(a)) has been reconstructed as shown in figure 7(b), where the dashed line means the results of fitting to equation (8) and the horizontal line shows the 1.177 Å value. The constant k has been found equal to 3.168×10^{-3}. The critical value $r_{cr} = 1.128(4)$ Å coincides within the uncertainty limit with the ionic radius of samarium ion, which is in agreement with the experimentally observed instability of $SmGaO_3$. This consideration revealed that perovskite-type promethium oxide can be grown at ambient pressure.

The reconstructed phase diagram (figure 7(b)) is separated into three regions, where region 1 represents the range of compositions for compounds which undergo a structural phase transition $Pbnm$–$R\bar{3}c$. $LnGaO_3$ and their solid solutions with Ln average ionic radii and Δr values lying in region 3 cannot be synthesized at ambient pressure. High-quality single crystals can be obtained for compositions when Ln average ionic radii and Δr belong to region 2. The estimated rare-earth compositions in the pseudobinary system $Ln1GaO_3$–$Ln2GaO_3$, which satisfy region 2 are summarized in table 3. Therefore, only a narrow region of $LnGaO_3$ and their solid solutions with Ln ionic radii smaller than 1.177 Å could be applicable as potential substrates.

3.4. Surface energy

In addition to the conditions formulated by O'Bryan *et al* [62], we calculated the surface energy E_{surf} in $LnGaO_3$, which is also an important property for substrate materials. For this purpose a relative large slab of material was constructed and the surface energy was obtained via the relation

$$E_{surf} = \frac{E_{slab} - E_{bulk}}{2A}, \tag{9}$$

where E_{slab} is the energy of the slab, E_{bulk} is the energy of the identical amount of bulk material without the vacuum gap and A is the square of the surface. The procedure has been described in detail elsewhere [64]. The requirement of positive values for the surface energy serves as an independent control for the validity of the interaction model.

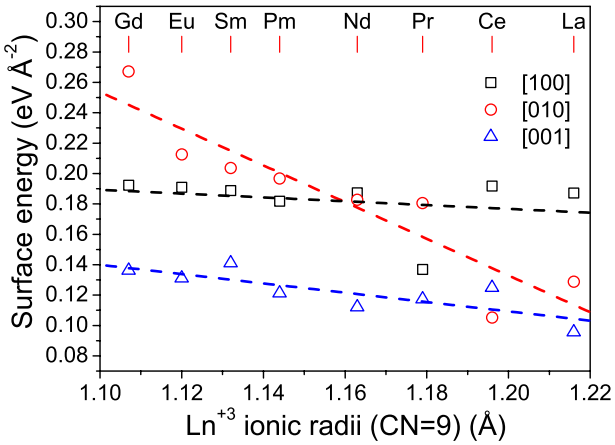

Figure 8. Calculated and linear fit of $LnGaO_3$ (Ln = La–Gd) surface energy at RT as a function of Ln^{3+} ionic radii for surfaces in principal crystallographic directions.

Calculations were performed for surfaces in the principal crystallographic directions of the crystal. The results of calculations are presented in figure 8. With decreasing Ln^{3+} ionic radii an increasing surface energy (e.g. adhesion) was observed for all surface orientations considered (the dashed lines correspond to fits), i.e. the deposition process is energetically favoured for $LnGaO_3$ with small Ln^{3+} ionic radii.

4. Conclusions

$LnGaO_3$ (Ln = La–Gd) thermal properties (dielectric constants, thermal expansion coefficients, phonon density of states and its projections, heat capacity and entropy, elastic moduli, Grüneisen parameters and Debye temperatures) were studied using atomistic simulation and the static lattice minimization method. For Pm, Sm, Eu and Gd orthogallates, the above-mentioned properties were predicted. Previous force field parameters [18, 47] were improved and supplemented for the present compounds. In spite of the rather simple model, a good description of interatomic interactions was observed, as indicated by the agreement between observed and calculated physical properties. Perovskite-type $LnGaO_3$ (Ln = La–Gd) materials were examined for compliance to conditions for substrates formulated by O'Bryan *et al* [62]. By analysing the calculated dielectric properties it was concluded that $LnGaO_3$ could be successfully used in HTSC microwave integrated circuits at operating frequencies below 10 GHz. Considering the total phonon DOS and its projections onto atomic species, it was concluded that $LnGaO_3$ (Ln = La–Gd), similarly to $NdGaO_3$ [18], $Nd_{0.75}Sm_{0.25}GaO_3$ [47] and $MgSiO_3$ [93], cannot be considered as Debye-like solids. Furthermore, it was concluded that rare-earth, gallium and oxygen atoms dominate the phonon spectrum in different frequency regions. Moreover, the Ln^{3+} region of contribution to the total DOS is shifted to the low-frequency part of the spectrum with increasing Ln^{3+} atomic number and, correspondingly, atomic weight. This shift causes the decrease of the Debye temperature, the heat capacity, the entropy, the Grüneisen parameter and TECs in $LaGaO_3$–$GdGaO_3$. It was concluded that $LnGaO_3$ (Ln = La–Gd) and its solid solutions with average Ln^{3+} ionic radii r_{Ln} in a nine-fold coordination sphere smaller than ∼1.177 Å are likely to be synthesized without micro-twins. On the other hand for $LnGaO_3$ and their solid solutions with average rare-earth ionic radii smaller than r_{Nd} the stabilization of the corresponding $Ln_3Ga_5O_{12}$ and $Ln_4Ga_2O_9$

phases becomes more preferable. High-pressure synthesis methods result in a substantial increase of the $LnGaO_3$ cost and are unable to provide single crystals of reasonable size. The assumption of a critical deformation describes such an instability, and by including the differences between rare-earths in pseudobinary systems $Ln1GaO_3$–$Ln2GaO_3$ the narrow region of $LnGaO_3$ (Ln = La–Gd) and its solid solutions applicable for substrates has been estimated.

Acknowledgments

This work was partially supported by grant of Ukrainian Ministry of Education and Science (project 'Cation'). AS gratefully acknowledges financial support from the Deutscher Akademischer Austauschdienst (German Academic Exchange Service). JDG would like to thank the Government of Western Australia for a Premier's Research Fellowship. Also, we would like to thank Artem R Oganov for helpful comments.

References

[1] Mogro-Campero A, Turner L G, Hall E L, Garbauskas M I and Lewis N 1989 *Appl. Phys. Lett.* **54** 2719
[2] Sandstrom R L, Giess E A, Gallaher W J, Segmuller A, Cooper E I, Chisholm M F, Gupta A, Shinde S and Laibowitz R B 1988 *Appl. Phys. Lett.* **53** 1874
[3] Mamutin V V, Toropov A A, Kartenko N F, Ivanov S V, Wagner A and Monemar B 1999 *Mater. Sci. Eng.* B **59** 56
[4] Feng M and Goodenough J B 1994 *J. Solid State Inorg. Chem.* **31** 663
[5] Petric A and Huang P 1996 *Solid State Ion.* **92** 113
[6] Liu Z G, Cong L G, Huang X Q, Lu Z and Su W H 2001 *J. Alloys Compounds* **314** 281
[7] Ishihara T, Furutani H, Arikawa H, Honda M, Akbay T and Takita Y 1999 *J. Electrochem. Soc.* **146** 1643
[8] Podlesnyak A, Rosenkranz S, Fauth F, Marti W, Sheel H J and Furrer A 1994 *J. Phys.: Condens. Matter* **6** 4099
[9] Podlesnyak A, Rosenkranz S, Fauth F, Marti W, Furrer A, Mirmelstein A and Sheel H J 1993 *J. Phys.: Condens. Matter* **5** 8973
[10] Marti W, Fischer P, Altorfer F, Scheel H J and Tadin M 1994 *J. Phys.: Condens. Matter* **6** 127
[11] Marti W, Medarde M, Rosenkranz S, Fischer P, Furrer A and Klemenz C 1955 *Phys. Rev.* B **52** 4275
[12] Marti W, Fischer P, Schefer J and Kubel F 1996 *Z. Kristallogr.* **221** 891
[13] Savytskii D, Vasylechko L, Senyshyn A, Matkovskii A, Bähtz C, Sanjuan M L, Bismayer U and Berkowski M 2003 *Phys. Rev.* B **68** 024101
[14] Slater P R, Irvine J T S, Ishihara T and Takita Y 1998 *J. Solid State Chem.* **139** 135
[15] Howard C J and Kennedy B J 1999 *J. Phys.: Condens. Matter* **11** 3229
[16] Lerch M, Boysen H and Hansen T 2001 *J. Phys. Chem. Solids* **62** 445
[17] Vasylechko L, Pivak Ye, Senyshyn A, Savytskii D, Berkowski M, Borrmann H, Knapp M and Paulmann C 2005 *J. Solid State Chem.* **178** 270
[18] Senyshyn A, Vasylechko L, Knapp M, Bismayer U, Berkowski M and Matkovskii A 2004 *J. Alloys Compounds* **382** 84
[19] Chaix-Pluchery O, Chenevier B and Robles J J 2005 *Appl. Phys. Lett.* **86** 251911
[20] Tanaka M, Shishido T, Horiuchi H, Toyota N, Shindo D and Fukuda T 1993 *J. Alloys Compounds* **192** 87
[21] Shishido T, Zheng Y, Saito A, Horiuchi H, Kudou K, Okada S and Fukuda T 1997 *J. Alloys Compounds* **260** 88
[22] Stan M, Armstrong T J, Butt D P, Wallace T C, Park Y S, Haertling C, Hartmann T and Hanrahan R J 2002 *J. Am. Ceram. Soc.* **85** 2811
[23] Vasylechko L, Niewa R, Senyshyn A, Pivak Ye, Savytskii D, Knapp M and Bähtz C 2002 *Hasylab Ann. Rep.* **1** 223
[24] Vasylechko L, Niewa R, Schnelle W, Senyshyn A and Knapp M 2003 *Proc. 9th European Conf. on Solid State Chemistry (Stuttgart)* p 49
[25] Vasylechko L O and Senyshyn A T 2004 *Visnyk Lviv Polytech.* **513** 3
[26] Vasylechko L, Fadyeev S V, Red'ko N and Berkowski M 2002 *Visnyk Lviv Polytech.* **455** 21
[27] Aleksiyko R, Berkowski M, Byszewski P, Dabrowski B, Diduszko R, Fink-Finowicki J and Vasylechko L O 2001 *Cryst. Res. Technol.* **36** 789

[28] Vasylechko L O, Red'ko N A, Savytskii D and Fadyeev S V 2000 *Visnyk Lviv Polytech.* **401** 57
[29] Vasylechko L, Niewa R, Borrmann H, Knapp M, Savytskii D, Matkovskii A, Bismayer U and Berkowski M 2001 *Solid State Ion.* **143** 219
[30] Vasylechko L, Matkovski A, Suchocki A, Savytskii D and Syvorotka I 1999 *J. Alloys Compounds* **286** 213
[31] Islam M S and Davies R A 2004 *J. Mater. Chem.* **14** 86
[32] Arseniev P A, Covba L M, Bagdasarov H S, Dzhurynskii B F, Potemkin A V, Pokrovskii B I, Spiridonov F M, Antonov V A and Iluhin V V 1983 *The Rare-Earth Compounds. Systems with I–III Groups Elements Oxides* (Moscow: Nauka) (in Russian)
[33] Ito K, Tezuka K and Hinatsu Y 2001 *J. Solid State Chem.* **157** 173
[34] Levy M R, Grimes R W and Sickarus K E 2004 *Phil. Mag.* **84** 533
[35] Marezio M, Remeika J P and Dernier P D 1968 *Inorg. Chem.* **7** 1337
[36] Geller S, Curlander P J and Ruse G F 1974 *Mater. Res. Bull.* **9** 637
[37] Guitel J C, Marezio M and Mareschal J 1976 *Mater. Res. Bull.* **11** 739
[38] Lufaso M W and Woodward P M 2001 *Acta Crystallogr.* B **57** 725
[39] Minervini L, Zacate M O and Grimes R W 1999 *Solid State Ion.* **116** 339
[40] Bush T S, Gale J D, Catlow C R A and Battle P D 1994 *J. Mater. Chem.* **4** 1765
[41] Lewis G V and Catlow C R A 1985 *J. Phys. C: Solid State Phys.* **18** 1149
[42] Battle P D, Bush T S and Catlow C R A 1995 *J. Am. Chem. Soc.* **117** 6292
[43] Cherry M, Islam M S and Catlow C R A 1995 *J. Solid State Chem.* **118** 125
[44] Woodley S M, Battle P D, Gale J D and Catlow C R A 2003 *Chem. Mater.* **15** 1669
[45] Milanese C, Buscaglia V, Maglia F and Anselmi-Tamburini U 2004 *Chem. Mater.* **16** 1232
[46] Williford R E, Stevenson J W, Chou S Y and Pederson L R 2001 *J. Solid State Chem.* **156** 394
[47] Senyshyn A, Oganov A R, Vasylechko L, Ehrenberg H, Bismayer U, Berkowski M and Matkovskii A 2004 *J. Phys.: Condens. Matter* **16** 253
[48] Vasylechko L, Berkowski M, Matkovski A, Savytskii D and Fink-Finowicki J 2000 *Mater. Res. Bull.* **35** 333
[49] Vasylechko L, Berkowski M, Matkovskii A, Piekarczyk W and Savytskii D 2000 *J. Alloys Compounds* **300/301** 471
[50] Berkowski M, Fink-Finowicki J, Piekarczyk W, Perchuc L, Byszewski P, Vasylechko L O, Savytskii D I, Mazur K, Sass J, Kowalska E and Kapusniak J 2000 *J. Cryst. Growth* **209** 75
[51] Berkowski M, Fink-Finowicki J, Byszewski P, Diduszko R, Kowalska E, Aleksiyko R, Piekarczyk W, Vasylechko L O, Savytskij D I, Perchuc L and Kapusniak J 2001 *J. Cryst. Growth* **222** 194
[52] Vasylechko L 2001 *Visnyk Lviv University (Chem. Series)* **40** 98
[53] Shannon R D 1976 *Acta Crystallogr.* A **32** 751
[54] Vasylechko L, Akselrud L, Morgenroth W, Bismayer U, Matkovskii A and Savytskii D 2000 *J. Alloys Compounds* **297** 46
[55] Krivchikov A I, Gorodilov B Ya, Kolobov I G, Erenburg A I, Savitskii D I, Ubizskii S B, Syvorotka I M and Vasilechko L O 2000 *J. Low Temp. Phys.* **26** 370
[56] Savytskii D 2004 private communication
[57] Belsky A, Hellenbrandt M, Karen V L and Luksch P 2002 *Acta Crystallogr.* B **58** 364
[58] Kantorovich L N 1995 *Phys. Rev.* B **51** 3520
Kantorovich L N 1995 *Phys. Rev.* B **51** 3535
[59] Gale J D 1996 *Phil. Mag.* B **73** 3
[60] Gale J D 1997 *J. Chem. Soc. Faraday Trans.* **93** 629
[61] Monkhorst H J and Pack J D 1976 *Phys. Rev.* B **13** 5188
[62] O'Bryan H M, Gallaher P K, Berkstresser G W and Brandle C D 1990 *J. Mater. Res.* **5** 183
[63] Hollmann E K, Vendik O G, Zaitsev A G and Melekh B T 1994 *Supercond. Sci. Technol.* **7** 609
[64] Gale J D and Rohl A L 2003 *Mol. Simul.* **29** 291
[65] Konaka T, Sato M, Asano H and Kubo S 1991 *J. Supercond.* **4** 283
[66] Savytskii D I, Ubizskii S B, Matkovskii A O, Suchocki A, Bismayer U, Pashkov V M, Borisov V N, Alexandrovskii A N and Soldatov A V 1999 *Phase Transit.* A **70** 57
[67] Konopka J and Wolff I 1992 *IEEE Trans. Microw. Theory Tech.* **40** 2418
[68] Cho S Y, Kim I T and Hong K S 1999 *J. Mater. Res.* **14** 114
[69] Dube D C, Sheel H J, Reaney I, Daglish M and Setter N 1994 *J. Appl. Phys.* **75** 4126
[70] Sasaura M, Mukaida M and Miyazawa S 1990 *Appl. Phys. Lett.* **57** 2728
[71] Kim M H, Nahm S, Choi C H, Lee H J and Park H M 2002 *Japan. J. Appl. Phys.* **41** 717
[72] Krupka J, Geyer R G, Kuhn M and Hinken J H 1994 *IEEE Trans. Microw. Theory Tech.* **42** 1886
[73] Anderson O L 1995 *Equations of State for Solids in Geophysics and Ceramic Science* (Oxford: Oxford University Press)

[74] Efendiev G H and Karaev Z H 1962 *Azerb. Khim. Zh.* **5** 19
[75] Kennedy B J, Vogt T, Martin C D, Parise J B and Hriljac J A 2001 *J. Phys.: Condens. Matter* **13** L925
[76] Robie R A and Edwards J L 1966 *J. Appl. Phys.* **37** 2569
[77] Senyshyn A, Kraus H, Mikhailik V B and Yakovyna V 2004 *Phys. Rev.* B **70** 214306
[78] Zinkevich M, Geupel S, Nitsche H, Ahrens M and Aldinger D 2004 *J. Phase Equilib. Diff.* **25** 437
[79] Schnelle W, Fischer R and Gmelin E 2001 *J. Phys. D: Appl. Phys.* **34** 846
[80] Miyazawa S 1989 *Appl. Phys. Lett.* **55** 2230
[81] Tompsett G A, Sammes N M and Phillips R J 1999 *J. Raman Spectrosc.* **30** 497
[82] Sasaura M and Miyazawa S 1992 *J. Cryst. Growth* **123** 126
[83] Miyazawa S, Sasaura S and Mukaida M 1993 *J. Cryst. Growth* **128** 704
[84] Sasaura M and Miyazawa S 1997 *Defects Diffus. Forum* **150** 35
[85] Senyshyn A, Vasylechko L, Savytskii D, Bähtz C, Knapp M, Bismayer U and Berkowski M 2002 *Hasylab Ann. Rep.* **1** 355
[86] Kobayashi J, Tazoh Y, Sasaura M and Miyazawa S 1991 *J. Mater. Res.* **6** 97
[87] Sasaura M and Miyazawa S 1993 *J. Cryst. Growth* **131** 413
[88] Nicolas J, Coutures J and Coutures J P 1983 *Rev. Int. Hautes Temp. Refract.* **20** 129
[89] Nicolas J, Coutures J, Coutures J P and Boudot B 1984 *J. Solid State Chem.* **52** 101
[90] Ross N L, Zhao J and Angel R J 2004 *J. Solid State Chem.* **177** 1276
[91] Ross N L, Zhao J and Angel R J 2004 *J. Solid State Chem.* **177** 3768
[92] Kitaigorodskiy A I 1983 *Mixed Crystals* (Moscow: Nauka) (in Russian)
[93] Oganov A R, Brodholt J P and Price G D 2000 *Phys. Earth Planet. Inter.* **122** 277